



# From Bad Electrochemical Practices to an Environmental and Waste Reducing Approach for the Generation of Active Hydrogen Evolving Electrodes

Lisa Ring, Bruno G. Pollet, Marian Chatenet, Sofyane Abbou, Karsten Küpper, Mercedes Schmidt, Marten Huck, Aurelia Gries, Martin Steinhart, and Helmut Schäfer\*

**Abstract:** The electrodeposition of noble metals using corresponding dissolved metal salts represents an interesting process for the improvement of the electrocatalytic hydrogen evolution reaction (HER) properties of less active substrate materials. The fact that only a small fraction of the dissolved noble metals reaches the substrate represents a serious obstacle to this common procedure. We therefore chose a different path. It was found that the HER activity of Ni42 alloy drastically increased ( $\eta = 140$  mV at  $j = 10$  mA cm<sup>-2</sup>; pH 1) when a platinum counter electrode was used during polarization experiments in acid. This improvement was caused by a platinum transfer from the platinum anode to the steel cathode, a process which occurred simultaneously to the hydrogen evolution. The negligible accumulation of Pt (26  $\mu$ g) in the electrolyte turns this straight-forward transfer procedure into a highly cost-effective, environmentally friendly, and waste reducing approach for the generation of cheap, stable and effective HER electrodes.

## Introduction

The ever-growing global energy demand of future societies can, in harmony with the environment, only be fulfilled by sustainable energy sources like thermal, sunlight, and wind. Solar energy can be stored in “chemical bonds”. This can be reasonably achievable by water electrolysis, using either a proton exchange membrane water electrolyzer (PEMWE) or an alkaline water electrolyzer (AWE), leading to the generation of the so-called solar fuels<sup>[1–9]</sup> which, in this case, consist of hydrogen (H<sub>2</sub>)—a promising energy carrier<sup>[5]</sup> and oxygen (O<sub>2</sub>).

Although hydrogen offers many advantages over other fuels, the cost for producing electrolytic hydrogen is rather high, with a current production price of €5–10/kg.<sup>[10]</sup> This price is related to the cost of electricity, and should be considered in addition to the capital cost (CAPEX) and operational cost (OPEX) of the electrolyzer; as most of PEMWEs use platinum-group metals (PGMs) such as iridium (Ir) and platinum (Pt), the PEMWE technology is inherently costly. PGMs and in particular Pt is used as it is the most effective electrocatalysts for the HER.<sup>[11,12]</sup> However, whilst Pt is characterized by its high-performance (low overpotential towards the HER), the metal is very expensive and thought to be scarce. Thus, there is still a need for developing cheap and easily accessible electrode materials that exhibit low overpotentials on the cathode side, allowing for efficient conversion of electrical energy into hydrogen gas through the HER.

The electrodeposition of a thin, highly HER active Pt layer on a conductive substrate represents one possible route on the way to such a desired material.

The conventional approach to electrodeposit Pt takes advantage of a Pt containing electrolyte achieved upon the dissolution of Pt salts. From experience, it has been observed that only a very small fraction of the platinum which was originally dissolved is transferred to the electrode (intended to be modified), which definitely lowers the cost-efficiency and the environmental friendliness of this approach. In our conditions we have been following a different path, allowing the decoration of Pt on stainless steel using a Pt counter electrode (CE) and a Ni42 steel working electrode (WE) in a water electrolysis reaction, carried out at a low pH value and in an electrolyte not containing any Pt salts initially. Generally, the use of a platinum CE for the evaluation of non-PGM based electrodes is well-known to be questionable, due to the risk of contaminating the WE with platinum,

[\*] L. Ring, M. Huck, A. Gries, Dr. H. Schäfer  
Institute of Chemistry of New Materials, The Electrochemical Energy and Catalysis group, University of Osnabrück  
Barbarastrasse 7, 49076 Osnabrück (Germany)  
E-mail: helmut.schaefer@uos.de

Prof. Dr. B. G. Pollet  
Hydrogen Energy and Sonochemistry Research group, Department of Energy and Process Engineering, Faculty of Engineering, Norwegian University of Science and Technology (NTNU)  
O-7491, Trondheim (Norway)

Prof. Dr. M. Chatenet, S. Abbou  
Univ. Grenoble Alpes, CNRS, Grenoble-INP (Institute of Engineering, Univ. Grenoble Alpes), LEPMI  
38000 Grenoble (France)

Dr. K. Küpper  
Department of Physics, Universität Osnabrück  
Barbarastrasse 7, 49076 Osnabrück (Germany)

Dr. M. Schmidt, Prof. M. Steinhart  
Institut für Chemie neuer Materialien, Universität Osnabrück  
Barbarastr. 7, 49076 Osnabrück (Germany)

Supporting information and the ORCID identification number(s) for the author(s) of this article can be found under:  
<https://doi.org/10.1002/anie.201908649>.

© 2019 The Authors. Published by Wiley-VCH Verlag GmbH & Co. KGaA. This is an open access article under the terms of the Creative Commons Attribution Non-Commercial NoDerivs License, which permits use and distribution in any medium, provided the original work is properly cited, the use is non-commercial and no modifications or adaptations are made.



**Figure 1.** Photo of the experimental setup taken before carrying out the polarization experiments in the absence and presence of ultrasound a) and whilst performing the first activation procedure b).

especially when positive potentials are applied to the Pt electrode.<sup>[13]</sup> However, in this work, we used this drawback to our advantage. Upon using this strategy (self-dissolution of Pt at high electrode potential for example,  $E > +1600$  mV vs. RHE) we could only detect a negligible amount of remaining platinum in the electrolyte used, clearly underpinning the 100% effectiveness of the platinum transfer process. The simultaneously occurring hydrogen evolution on the Ni42 stainless steel surface affected the electrodeposition of a homogeneous layer but was substantially suppressed upon applying ultrasonic energy (80 kHz, 48–72 W) to the electrolysis cell (the setup of which is shown in Figure 1). The decoration of Ni42 stainless steel with Pt by the ultrasonic and sonoelectrochemical approaches were found to be highly effective to render steel in a competitive hydrogen-evolving electrode without exhibiting the disadvantage of classically performed Pt decoration processes: The wastage of expensive platinum.

## Results and Discussion

### Silent conditions

Recently Schäfer and Chatenet showed that surface-modified (stainless) steel can be used as water splitting electrodes.<sup>[14]</sup> The approaches shown by Chatenet et al.<sup>[15]</sup> and Schäfer et al.<sup>[16–19]</sup> and by some of other groups are taking advantage of the elements contained in steel like Fe, Ni and Co, known for their sophisticated properties (at least) towards the electrocatalytically-initiated OER. However, scientists failed, likely owing to the absence of noble ingredients, in rendering steel at least as active towards the HER as Pt is.<sup>[14]</sup>

In this study, electrochemical decoration of Ni42 stainless steel with platinum was realized in 0.05 M sulfuric acid

(initially free of any dissolved Pt species) by using a three-electrode set up consisting of a stainless steel Ni42 WE, a platinum CE, and a reversible hydrogen electrode (RHE) as reference electrode (Figure 1). Platinum was transferred from the CE to the WE through a procedure consisting of repeated cycling (100 cycles) in the potential ( $E$ ) range 0.00 V vs. RHE and  $-0.40$  V vs. RHE ( $E$  of the Pt CE was at most  $+1.70$  V vs. RHE), followed by a galvanostatic long-term polarization procedure (Figure 2), resulting in Pt decorated Ni42 stainless steel henceforth referred to as “sample Ni42Pt”.

Figure 2a shows that larger currents to potential ratio are obtained upon cycling of the potential. After 100 voltammetry cycles, the current density reached  $-17$  mA cm<sup>-2</sup> at a potential of  $E = -400$  mV vs. RHE, a value that is ca. 2.5 times higher than that observed for untreated Ni42 (ca. 7 mA cm<sup>-2</sup>, Figure 2a).

This was confirmed under steady state conditions as the potential required to ensure  $-10$  mA cm<sup>-2</sup> current density decreased by 180 mV (from 370 mV overpotential to 190 mV overpotential) through 50 000 s of chronopotentiometry (Figure 2b). The contamination of a non-PGM-based working electrode by a Pt counter-electrode is a classical issue in electrocatalysis.<sup>[12]</sup> Thus, it was an indispensable prerequisite to replace the platinum counter electrode with a material that does not lead to any contamination of the working electrode, for example, graphite (Figure 3).

In comparison with non-activated Ni42 steel, Ni42Pt exhibited a substantial enhancement in HER activity (Figure 3, black and blue curves) at pH1 and pH0. The average potential after 50 000 s of chronopotentiometry was found to be  $-218$  mV vs. RHE ( $j = -10$  mA cm<sup>-2</sup>; 0.05 M H<sub>2</sub>SO<sub>4</sub>, Figure 3a, black curve) whereas non-treated Ni42 steel required an average potential of  $E = -335$  mV vs. RHE (Figure 3a, blue curve).

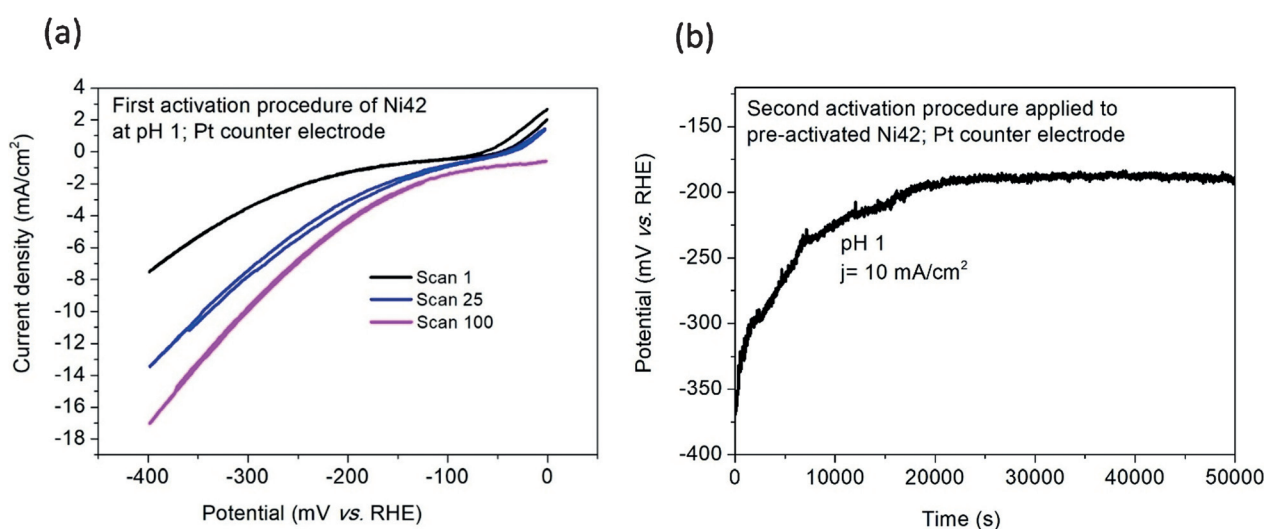


**Figure 2.** Electrochemical activation of Ni42 steel upon usage of a Pt counter electrode. a) First activation procedure based on a cyclic voltammetry experiment. b) Second activation procedure based on a chronoamperometry experiment.

The HER based current density realized at potential of  $E = -400$  mV vs. RHE was found to be  $-30 \text{ mA cm}^{-2}$  for pH 0 and  $-6 \text{ mA cm}^{-2}$  for pH 1 for the non-treated Ni42 samples and,  $-90 \text{ mA cm}^{-2}$  for pH 0 and  $-17.5 \text{ mA cm}^{-2}$  for pH1 for the sample Ni42Pt (Figures 3b and c). In any case, there is still a significant difference in overall HER performance at pH 0 or 1 between pure Pt (determined by us or other groups<sup>[20,21]</sup>) and sample Ni42Pt (Figures 3b and c) as can be taken from the substantial gap between the CV curves of samples Pt and Ni42Pt recorded at pH1 and pH0 (Figures 3b and c). Additionally, under our conditions, a substantial decrease of the HER activity for sample Ni42Pt under long-term measurements was observed (Figure 3a, black curve). For example the potential was found to increase by circa  $+80$  mV after 50000 s of chronopotentiometry carried out in 0.05 M sulfuric acid at  $j = -10 \text{ mA cm}^{-2}$  (Figure 3a, black curve). From these observations, it can be stipulated that two processes occur simultaneously on the surface of Ni42 steel during the first and second activation procedures (Figure 2), namely hydrogen ( $\text{H}_2$ ) bubble formation and Pt electrodeposition.<sup>[22]</sup>

Moreover, it turned out that the shift of the CV curves towards higher current density values with increased number of cycles (up to 100) as seen in Figure 2a, can only be achieved when the electrolyte volume, the magnetic stirring bar size, the stirring speed, and the electrode geometry (that is the distance between the Ni42 working electrode and the Pt counter electrode, and the distance between Ni42 and the reference electrode) are optimized. If too strong stirring is used, Pt species cannot diffuse/migrate from the Pt anode (counter electrode in OER and dissolution regime) to the Ni42 cathode (working electrode, in HER and Pt deposition regime). However, if the stirring is too weak,  $\text{H}_2$  bubbles are not released fast enough from the Ni42 working electrode surface and may affect the electrodeposition of Pt species.

### Ultrasonic conditions

In order to overcome and circumvent these problems, ultrasonication (80 kHz, 48–72 W) was used. Ultrasonication applied to electrochemically promoted reactions is known to not only influence gas bubble removal from surfaces but also offers many other advantages.<sup>[23,24]</sup> An increase in electrode cleanliness, metal depassivation, and enhanced mass-transport of electroactive species to the electrode surface will result in enhanced electrochemical diffusion processes, in an increase in a) electrochemical rates and yields, b) process efficiencies, as well as in a decrease of electrode overpotentials; this overall leads to improved electroplated and electrodeposited materials (hardness, porosity, and thickness).<sup>[25]</sup>

We would like to emphasize at this point that we employed ultrasound solely for the fabrication of the HER electrode and not when the ready-made electrode was used as a hydrogen forming electrode. Thus, we would like to address questions whether ultrasound affects for example, electron transfer kinetics<sup>[23]</sup> in an additional contribution.

Ultrasonic-assisted two steps cyclic voltammetry activation followed by ultrasonic-assisted chronopotentiometry was applied to Ni42 (see Supporting Information), both performed using a platinum counter electrode (Figure 4).

Whereas 100 CV cycles were required in the absence of ultrasound to reach a current density of circa  $-17 \text{ mA cm}^{-2}$  (Figure 2(a), this value was obtained after only 30 CV cycles when the electrolysis cell was under ultrasonic treatment (80 kHz, 48 W) (Figure 4a). After 65 CV scans ( $j = -34 \text{ mA cm}^{-2}$  at  $E = -400$  mV vs. RHE) ultrasonic-assisted activation step I), an intermediate step was added to clean the platinum electrode for 60 min in a water ultrasonic bath, before polarization experiments were continued (ultrasonically-assisted activation step II; 80 kHz, 72 W Figure 4b). The current density reached  $-46 \text{ mA cm}^{-2}$  after further 35 CV scans (Figure 4b). An additional step (ultrasonic assisted activation step III) consisting of ultrasonically-assisted chro-

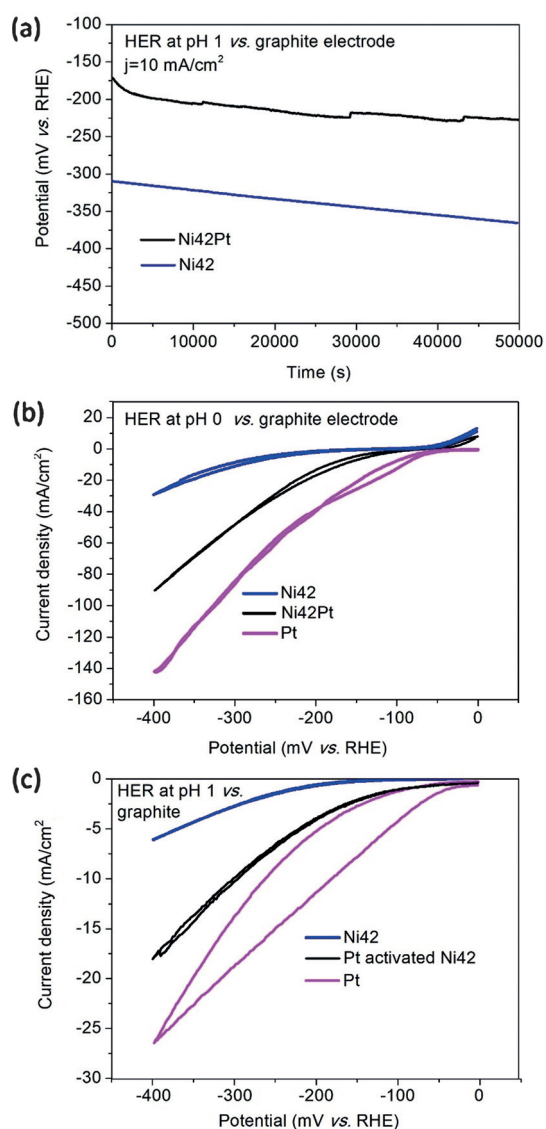


**Figure 3.** The electrochemical HER properties of Ni42 stainless steel decorated (or not) with Pt at pH 0 and pH 1 evaluated upon usage of graphite as counter electrode and compared with noble HER benchmarks. a) Comparison of the steady state HER performance (pH 1) of samples Ni42 and Ni42Pt. b) Comparison of the non-steady state HER performance (pH0) of platinum with samples Ni42 and Ni42Pt. c) Comparison of the non-steady state HER performance (pH 1) of platinum with samples Ni42, and Ni42Pt.

nopotentiometry performed in the presence of a Pt counter electrode which ends up in sample Ni42SoPt, turned out to be efficient in order to improve the stability of the HER catalyst (Supporting Information, Figure S1). Long-term polarization experiments with a graphite counter electrode reveal Ni42-SoPt as a highly active and highly stable HER electrode in an acidic medium (Figure 5a).

Sample Ni42SoPt exhibits the best electrocatalytic HER properties of all platinum-activated Ni42 samples. Exhibiting a current density of  $j = -25 \text{ mA cm}^{-2}$  at  $-400 \text{ mV vs. RHE}$  (Ni42Pt,  $j = -17.5 \text{ mA cm}^{-2}$ ), Ni42SoPt outperforms sample Ni42Pt and was found to be nearly *on par* with the one for pure platinum ( $j = -26.3 \text{ mA cm}^{-2}$ ; Figure 5b). A quantita-

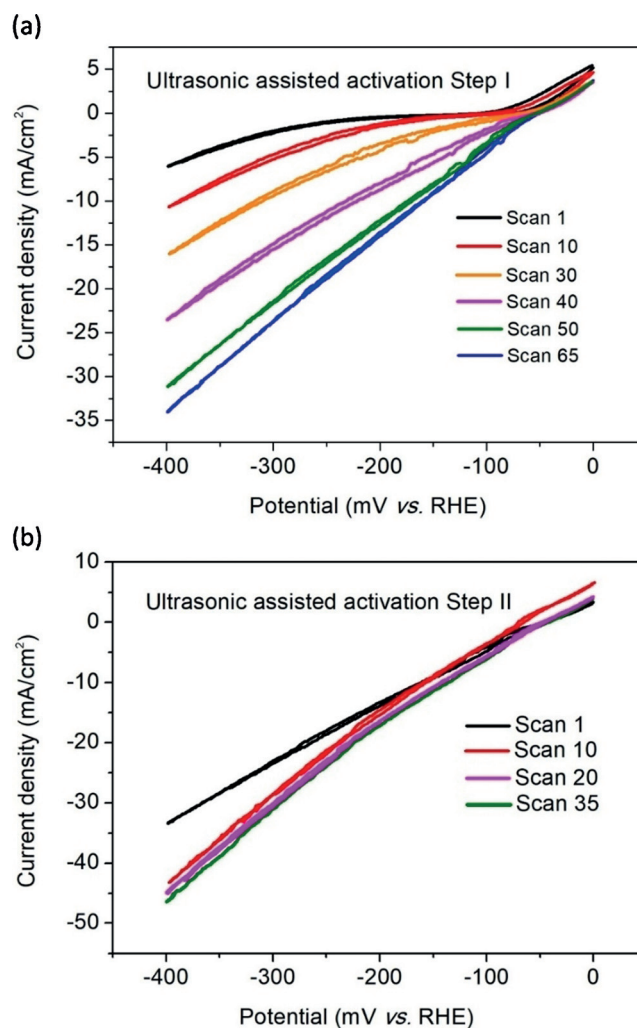


**Figure 4.** Ultrasonically assisted electrochemical activation of Ni42 stainless steel upon usage of a Pt counter electrode, ultrasonic frequency: 80 kHz. a) First activation procedure consisting of ultrasonically assisted (80 kHz, 48 W) 65 cyclic voltammetry scans. b) Second activation procedure consisting of ultrasonically-assisted (80 kHz, 72 W) 35 cyclic voltammetry scans.

tive charge to hydrogen conversion rate (99.9%) was determined for the electrocatalytically initiated hydrogen evolution upon sample Ni42SoPt (Figure 5c and Supporting Information). A potential industrial implantation of our Ni42SoPt electrode (PEM electrolyzer with 120 cells, each of them  $20 \times 20 \text{ cm}$ ) with a total electrode area of  $4.8 \text{ m}^2$ , would theoretically result in a production rate of  $6.14 \text{ m}^3 \text{ H}_2 \text{ h}^{-1}$  at  $20^\circ \text{C}$ , at  $j = 300 \text{ mA cm}^{-2}$  and  $\text{FE} = 95\%$ . As expected, sample Ni42SoPt exhibited, not only in  $0.05 \text{ M H}_2\text{SO}_4$  but also in  $0.5 \text{ M H}_2\text{SO}_4$ , a very close HER performance ( $E = -400 \text{ mV vs. RHE}$  at  $j = -125 \text{ mA cm}^{-2}$ ) compared to pure platinum (sample Pt;  $E = -400 \text{ mV vs. RHE}$  at  $j = -140 \text{ mA cm}^{-2}$ ; Figure 5d). In the high current density range ( $-10 < j < -150 \text{ mA cm}^{-2}$ ), a Tafel slope was found to be  $191 \text{ mV dec}^{-1}$  (Supporting Information, Figure S2). The Tafel slope for Pt in the same current density region amounted to  $109 \text{ mV dec}^{-1}$  (Ni42:  $201 \text{ mV dec}^{-1}$ ; Ni42Pt:  $206 \text{ mV dec}^{-1}$ ; Supporting Information, Figure S2). Pure platinum shows

better HER performance at high current densities than Ni42SoPt. We claim that the differences in Tafel slopes are due to different physicochemical properties of the surfaces

(for example, hydrophobicity, porosity) which influence bubble adhesion/detachment. However, the HER performance (under laboratory conditions) can be seen as competitive to recently-developed electrocatalysts<sup>[26,27]</sup> as well as commercially available ones.<sup>[28,29]</sup> For example, Popczun et al.<sup>[27]</sup> recently reported that nano-scaled Ni<sub>2</sub>P exhibited highly-active and stable electrocatalytically initiated hydrogen evolution. In their conditions, Ni<sub>2</sub>P nanoparticles were synthesized in high boiling organic solvent (1-octadecene, oleylamine, and tri-n-octylphosphine) and deposited on titanium foil with a catalyst (Ni<sub>2</sub>P) loading of 10 μgmm<sup>-2</sup>. The potential required for  $j = -10 \text{ mA cm}^{-2}$  HER based current density derived from steady-state measurements amounted to  $-115 \text{ mV vs. RHE}$  in 0.5 M sulfuric acid. A flat electrode consisting of metal ion containing triazine thiolate modified copper was recently introduced by Vishwanath et al.<sup>[30]</sup> and turned out to be substantially weaker (HER-) active ( $E = -270 \text{ mV vs. RHE}$  at  $j = -10 \text{ mA cm}^{-2}$  in 0.5 M H<sub>2</sub>SO<sub>4</sub>) than our modified stainless steel. Co<sub>2</sub>P nanowires generated upon a microwave-assisted approach showed, at given potential, competitive current densities ( $E = -110 \text{ mV vs. RHE}$  at  $j = -10 \text{ mA cm}^{-2}$ ).<sup>[31]</sup> Based on Tafel measurements Ma et al. determined for commercial Pt/C with a loading of around 50 μgcm<sup>-2</sup> at  $\eta \approx 35 \text{ mV}$ , a HER based current density of  $-1.6 \text{ mA cm}^{-2}$ <sup>[28]</sup> which represents an activity below the one of Ni42SoPt ( $j = -7 \text{ mA cm}^{-2}$  at  $\eta = 40 \text{ mV}$ ; Supporting Information, Figure S2). It should be mentioned, that in contrary to our steel-based electrodes, Pt/C as well as the electrode consisting of Co<sub>2</sub>P nanowires cannot be seen as a flat one, leading to a projected surface area significantly lower than the real surface area; thus, the high current density monitored cannot be directly compared with those derived from flat electrodes. This also explains why the overpotential at given current densities, reported in some contributions for porous materials, is even lower than the one that is assigned to pure platinum. Therefore, the HER onset potential seems to be a more meaningful HER activity parameter and here platinum (smooth) metal still can be seen as the benchmark.<sup>[32]</sup> With respect to the onset of hydrogen evolution ( $E_{\text{onset}} = \text{potential to ensure a HER based current density of } -0.25 \text{ mA cm}^{-2}$ ) in pH 1 regime our modified steel Ni42SoPt is highly competitive ( $-14 \text{ mV vs. RHE}$ ) to platinum metal ( $-12 \text{ mV vs. RHE}$ ; Figure 5 b,d, Table 1) and substantially better than samples Ni42 ( $E_{\text{onset}} = -160 \text{ mV vs. RHE}$ ) and Ni42Pt ( $E_{\text{onset}} = -32 \text{ mV vs. RHE}$ ).

To sum up: Whereas under laboratory conditions (current density up to 50 mA cm<sup>-2</sup>) Pt modified Ni42 steel is *on par* with Pt (Figure 5) under industrial conditions ( $j >$

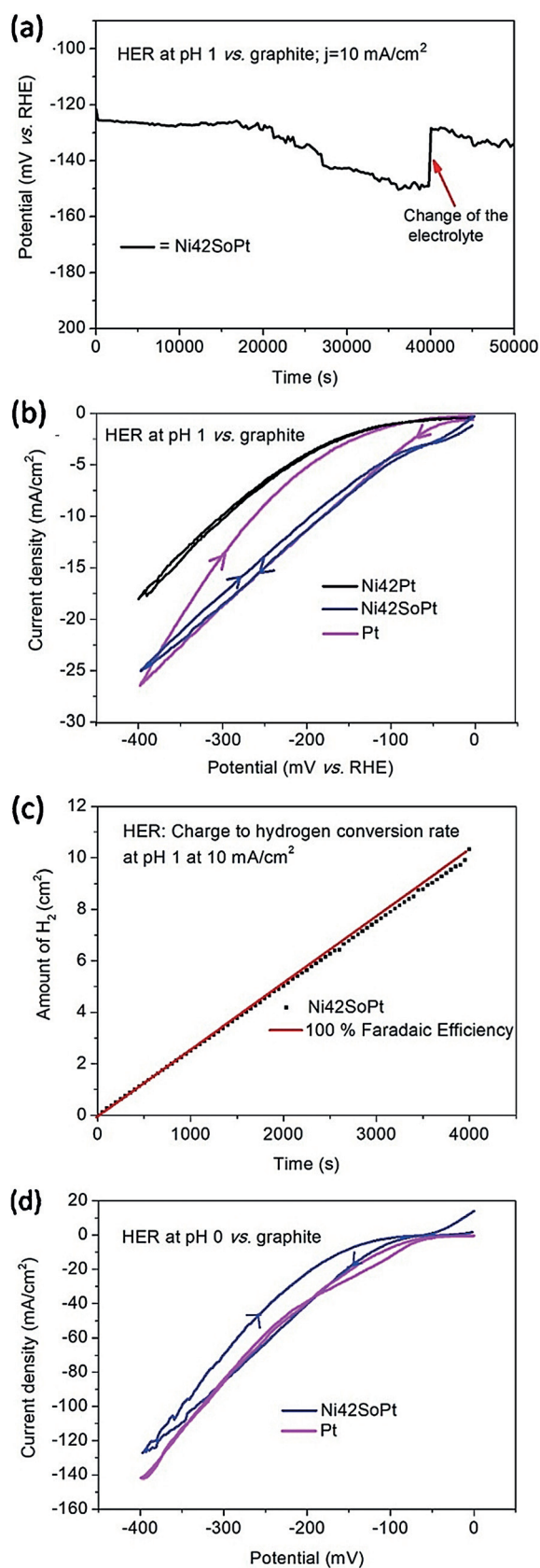


**Figure 5.** The HER performance of sample Ni42SoPt determined versus a graphite electrode. a) The steady state HER performance (pH 1) of Ni42SoPt. b) The non-steady state HER performance (pH 1) of Ni42SoPt. c) Determination of the charge to hydrogen conversion rate for the HER on sample Ni42SoPt based on a chronopotentiometry scan. The red line corresponds to 100% Faradaic efficiency (FE). The FE determined after 4000 s amounted to 99.9%. d) Comparison of the non-steady state HER performance (pH0) of platinum with sample Ni42SoPt.

**Table 1:** Overview of the steady state and non-steady state HER based electrochemical measurements, as well as the results from AFM testing carried out with samples Ni42, Ni42Pt, Ni42SoPt, and Pt.

| Sample   | Onset potential derived from cyclic-voltammetric measurements at $j = -0.25 \text{ mA cm}^{-2}$ |                 | Averaged overpotential required for $j = 10 \text{ mA cm}^{-2}$ based on Chronopotentiometry measurements |        | Tafel slope pH 0 [mV dec <sup>-1</sup> ] | $C_{dl}$ pH 1 [mF cm <sup>-2</sup> ] | Projected area (PA) surface area (SA) and average roughness (AR) as derived from AFM |
|----------|---|-----------------|---|--------|--|--------------------------------------|--|
|          | pH 1  | pH 0            | pH 1  | pH 0   |  |                                      |  |
| Ni42     | -160 mV vs. RHE   | -140 mV vs. RHE | 335 mV  | 306 mV | 328                                      | 6.8                                  | PA = 99.9 $\mu\text{m}^2$<br>SA = 101.8 $\mu\text{m}^2$<br>AR = 71.5 nm              |
| Ni42Pt   | -32 mV vs. RHE  | -28 mV vs. RHE  | 218 mV  | 99 mV  | 326                                      | 2.7                                  | PA = 100.062 $\mu\text{m}^2$<br>SA = 132.3 $\mu\text{m}^2$<br>AR = 98 nm             |
| Ni42SoPt | -14 mV vs. RHE  | -9 mV vs. RHE   | 140 mV  | 88 mV  | 291                                      | 4.35                                 | PA = 100.062 $\mu\text{m}^2$ ; SA = 131.4 $\mu\text{m}^2$<br>AR = 98 nm              |
| Pt       | -12 mV vs. RHE  | -7 mV vs. RHE   | 122 mV  | 81 mV  | 148                                      | -                                    | -  |

50 mA cm<sup>-2</sup>) there is still a gap between Ni42SoPt and pure Pt (Supporting Information, Figure S2).

Different coatings (nickel-iron alloy, SiO<sub>2</sub>, TiO<sub>2</sub>, ZrO<sub>2</sub>, AlOOH) applied to steel aiming in the improvement of its HER properties have been described in the literature.<sup>[33,34]</sup> However, the studies lack long-term stability measurements. Relatively recent studies exhibited HER activities which are far from those observed using PGM.<sup>[35]</sup> Furthermore, to the best of our knowledge, the majority of approaches shown in the literature focuses on the development of active and durable HER electrodes in alkaline media when PEMWEs<sup>[35-38]</sup> require OER and HER electrodes that are active and stable at low pH values. In particular, the stability criteria at low pH is difficult to reach. However, thin layers of PGMs deposited on steel are known to significantly improve the corrosion resistance of steel due to passivation.<sup>[39]</sup>

In order to shed further light on the HER mechanisms on our prepared electrodes and confirm successful decoration of Pt on Ni42 steel, we investigated the surface of Ni42SoPt by means of SEM (Figures 6a, b, c and d) and AFM (Figure 6e). Top view SEM (Figure 6a) and AFM (Figure 6e) images confirmed that the roughness of Ni42 steel (average roughness 71.5 nm)<sup>[40]</sup> was not substantially increased upon the chosen surface modification (Ni42SoPt: 98 nm). Double layer capacity investigations have been carried out with samples Ni42, Ni42Pt, and Ni42SoPt (Supporting Information, Figures S3-S8). An unusual high double-layer capacitance was determined for all samples (Ni42: 6.8 mF cm<sup>-2</sup>, Ni42Pt: 2.7 mF cm<sup>-2</sup>, Ni42SoPt: 4.35 mF cm<sup>-2</sup>). Values in the mF cm<sup>2</sup> range were also obtained for surface modified S235 steel as reported by us in one of our previous contributions.<sup>[41]</sup> However, phosphorized S235 steel exhibited substantially higher double-layer capacitance values (46.1 mF cm<sup>-2</sup>) than untreated S235 steel (0.2 mF cm<sup>-2</sup>),<sup>[41]</sup> which was very likely caused by the enormous increase of the porosity that occurs to steel S235 when phosphorized at high temperatures. Thus, we stipulate that the double layer capacitance values derived from samples Ni42, Ni42Pt, and Ni42SoPt, which are of the same order of magnitude, basically result from comparable roughness of samples Ni42, Ni42Pt, and Ni42SoPt; as confirmed by AFM and SEM techniques (Figure 6). Table 1

gives an overview of the electrochemical properties of samples Ni42, Ni42Pt, Ni42SoPt, and platinum, derived from non-steady-state and steady-state HER based measurements, it also compares the AFM results of samples Ni42, Ni42Pt, and Ni42SoPt. Elemental analysis of the surface of sample Ni42SoPt was obtained by X-ray energy-dispersive spectroscopy (XEDS; Figure 6a-d), and X-ray photoelectron spectroscopy (XPS; Figure 6f), respectively. Both methods confirmed the existence of Pt on the surface of sample Ni42SoPt. It was also observed that not only elemental platinum was found on the surface of sample Ni42SoPt: in addition to Pt<sup>0</sup>, platinum in oxidation state +2 was revealed (Figure 6f). A similar finding was recently reported by Yuan et al.<sup>[42]</sup>

The Pt 4f core level XPS consists of two peaks located at 71.3 (4f<sub>7/2</sub>) and 74.6 eV (4f<sub>5/2</sub>) on a binding energy scale. Whereas the 4f<sub>7/2</sub> core level energy is expected to be located at 70.7 eV for the metallic Pt "bulk" state of a polycrystalline Pt foil,<sup>[43]</sup> binding energies of 71.0 eV to 71.3 eV have been obtained for Pt electrodes with the platinum being in polycrystalline and nanostructured form.<sup>[44,45]</sup> The features, which we associate to metallic Pt (blue), show a rather pronounced tail (asymmetry) to higher binding energies (Figure 6f), another strong indication for metallicity. The analysis of the peak areas after background subtraction reveals that the platinum at the surface of sample comprises around 94.5 % metallic Pt (blue) and 5.5 % can be attributed to Pt(OH)<sub>2</sub> (green). The Pt 4f<sub>7/2</sub> binding energy of 72.2 eV found from the deconvolution for Pt(OH)<sub>2</sub> is in excellent agreement with the result for chemisorbed O/OH on Pt reported by Saveleva et al.<sup>[45]</sup>

These findings made us believe that platinum-oxide species are formed on the Pt counter electrode whilst HER on Ni42, for a given cell voltage of about 2.1 V (Pt: anode and Ni42: cathode), at  $E_{\text{cathode}} = -400 \text{ mV vs. RHE}$  ( $E_{\text{anode}} = +1700 \text{ mV vs. RHE}$ ). Thus, oxygen evolution took place on the Pt surface. Pioneering studies by the groups of Hoare, Bard, Bockris, and several others<sup>[46-48]</sup> showed that the cell voltage required to produce oxygen on a metallic surface is related to the redox potential of the metal/metal oxide couple, or in other words, even in the case of noble metals no oxygen

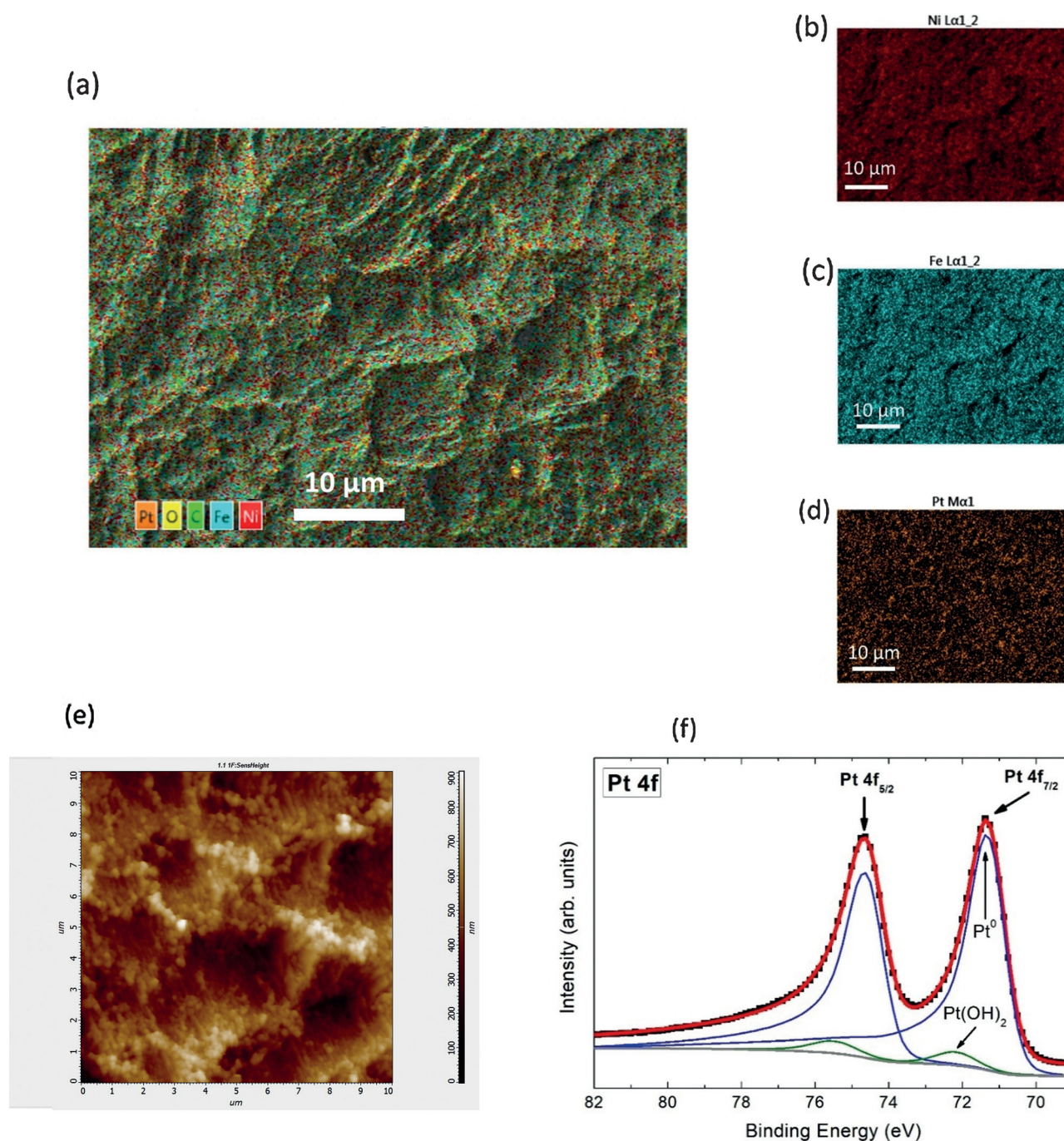


**Figure 6.** SEM, AFM, and XPS results of sample Ni42SoPt. Overlay image of a SEM picture with EDS data. Layered image combining 5 (Ni, Fe, Pt, O, C) maps (a). EDS maps of Ni (b), Fe (c) and Pt (d). AFM image of sample Ni42SoPt Sampling area: 100.062 μm μm. Height parameters: Root mean square roughness: 123.8 nm; Average roughness: 97.96 nm; Area peak-to-valley height: 902.1 nm; Maximum area peak height: 430.4 nm; Maximum area valley depth: 471.7 nm; Projected area: 100.062 μm<sup>2</sup>; Surface area: 131.4 μm<sup>2</sup> (e). High resolution Pt 4f x-ray photoelectron spectrum of sample Ni42SoPt (black points). The red line represents the result of the optimized fit. The de-convolution resulted in two 4f<sub>7/2</sub> peaks located at 71.3 eV (Pt<sup>0</sup>)<sup>[45]</sup> and 72.2 eV (Pt(OH)<sub>2</sub>)<sup>[45]</sup> and two 4f<sub>5/2</sub> peaks located at 74.6 eV (Pt<sup>0</sup>) and 75.6 eV (Pt(OH)<sub>2</sub>) binding energy, respectively (f).

can be released from the surface if the corresponding metal oxide is not formed.

Therefore, it is reasonable to assume that platinum oxide (PtO) is formed on the surface of the Pt counter electrode during the activation procedure leading to sample Ni42SoPt. Indeed, at potentials higher than +1 V vs. RHE in dilute

sulfuric acid, Pt initiates its surface (and then bulk) oxide formation, as well documented by the seminal work of Conway et al.<sup>[49–52]</sup> We claim herein that platinum oxide species formed on the Pt anode may be dissolved in the H<sub>2</sub>SO<sub>4</sub> and cationic Pt oxide species can be electrodeposited on the Ni42 steel (Figure 6 f). This assumption seems to be found-

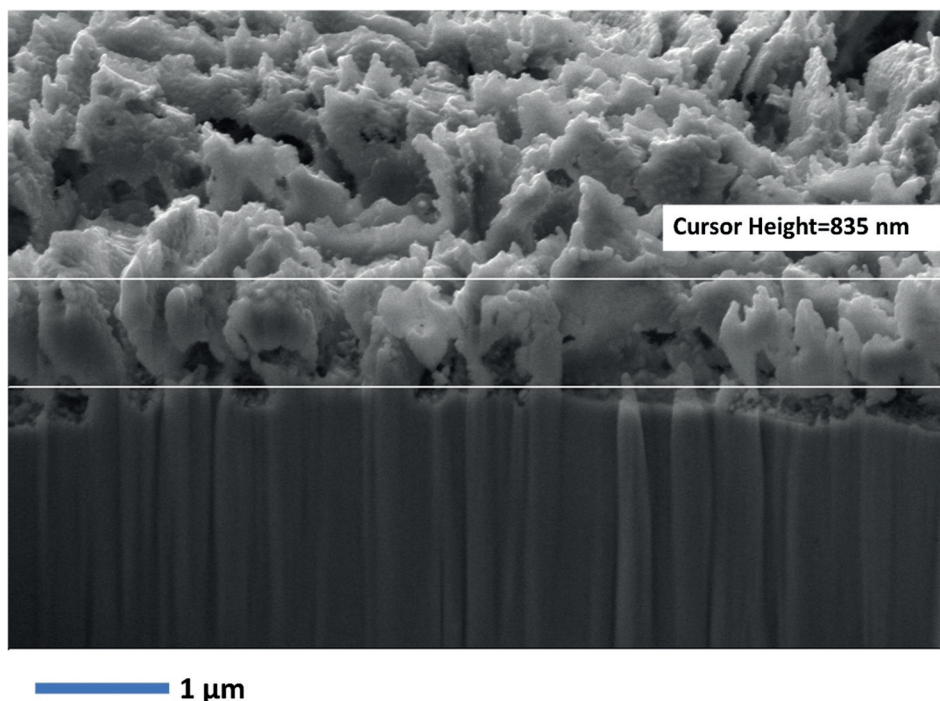


**Figure 7.** SEM image of a FIB machined cross section of sample Ni42SoPt. The rear wall of the trapezoidal trough is shown. This wall is orientated perpendicular to the surface of the specimen thus presenting a cross section of the sample. The accelerating voltage was adjusted to 7 kV and the SEM images were acquired using a secondary electron (SEI). Ion (Ga) beam settings: current: 240 pA, voltage: 7 kV, duration: 25 min.

ed<sup>[53–55]</sup> for example, Mitsushima et al.<sup>[53]</sup> investigated the dissolution of Pt in the presence of O<sub>2</sub> in sulfuric acid and postulated the following dissolution reaction:



The thickness of the Pt layer after the ultrasonically assisted activation steps I–III as determined by cross-sectional analysis amounted to circa 800–900 nm (Figure 7). Taking into account, the density of platinum of 21.45 g cm<sup>-3</sup> and the electrode area of 2 cm<sup>2</sup>, the total amount of platinum deposited on the Ni42 surface was calculated to be 3.65 mg based on a (fully) compact layer which agrees well with the mass loss of the Pt counter electrode that occurs whilst sample preparation. Based on five sample (Ni42SoPt) preparations the average mass loss of the Pt counter electrode amounted to 2.94 mg (for each sample produced) and the sum of the amount of Fe, Ni, and Pt dissolved in the electrolyte determined by ICP-MS technique was found to be 2.81 mg (Table 2). Notable is the extremely low amount of Pt (26 μg) in 100 mL of electrolyte. Thus, only 0.88 % of the 2.94 mg Pt (Pt mass loss of the CE) accumulates in solution, the rest is deposited. At first glance the absence of a mass increase of the Ni42 electrode during deposition (mass change: -3.22 mg) seems to be unusual. The analysis of the electrolyte reveals that the amount of Pt which is added to the Ni42 substrate (3.65 mg as mentioned above) is compensated by dissolution of Fe and Ni (Table 2). The Pt-decoration process is therefore likely (at least to some extent) to be a cementation (electroless) process, in which Pt<sup>II</sup> species originating from the

**Table 2:** Determination of the average mass loss of the platinum electrode (column I) and the average mass change of the Ni42 electrode (column II) based on 5 sample preparations. Determination of the amount of Pt deposited on the Ni42 steel based on the outcome of the FIB-SEM experiment (column III); Determination of the amount of ions dissolved in the electrolyte (column IV and V).

| I  | II  | III   | IV   | V   |
|--|---|---|--|---|
| Average mass loss of the Pt electrode [mg] | Average mass change of the Ni42 electrode occurring whilst decoration with Pt | Amount of Pt deposited on the Ni42 substrate* | Amount of transition metal ions dissolved in the electrolyte | Total amount of material dissolved in the electrolyte |
| 2.94 mg                                    | -3.22 mg  | 3.65 mg                                       | 0.026 mg [Pt]<br>1.60 mg [Fe]<br>1.18 mg [Ni]                | 2.81 mg   |

counter-electrode dissolution, play the role of oxidant at the Ni42 surface, leading to the preferential dissolution of Ni<sup>II</sup> or Fe<sup>II</sup>/Fe<sup>III</sup> species (Pt<sup>II</sup> + Ni → Ni<sup>II</sup> + Pt). The Pt loading (ca. 18 μg mm<sup>-2</sup>) is still below the lower limit compared to the loading of some commercially available electrodes<sup>[28,29,56]</sup> as Pt and Ir loadings in state-of-the art electrolyzers are in the range of 2–5 mg cm<sup>-2</sup>. For instance the loading for platinum black coated Nafion 115 from FuelCellsEtc used as cathode for PEMWE type electrolyzers amounts to 30 μg mm<sup>-2</sup>.<sup>[7]</sup> Recent studies have shown that lower Pt loadings can be feasible.<sup>[57]</sup> However, while Pt/C electrodes are inherently rather immune in HER conditions, this might not be the case when the electrolyzer operates in “start/stop” mode. In these



conditions, the “hydrogen electrode” would likely sweep between negative potentials (versus the RHE) in operation, and potentials as high as ca. +1 V vs. RHE in stop (in that case, air would likely intrude the whole cell). Alternation of the electrode potential on Pt/C electrocatalysts can be very detrimental, as Pt nanoparticles can catalyze the local corrosion of the carbon substrate, leading to restructuring of the active layer and loss of Pt nanoparticles (and of electrochemical surface area).<sup>[58–62]</sup> Such processes have been thoroughly studied for proton exchange membrane fuel cells,<sup>[63,64]</sup> and until now, been roughly disregarded in PEMWE. This could be a serious issue for PEMWE operated for the storage of renewable electricity (the present endeavor), and that the present solution brought herein (a carbon-free material), must not be subjected to such degradation.

## Conclusion

The use of a platinum counter electrode for the evaluation of non-PGM based electrodes is controversially discussed and questionable, due to the risk of contaminating the WE with platinum. However, such weak point of this experimental setup turned out to be of tremendous benefit for the generation of a highly active and stable HER electrocatalyst. We used a simple three-electrode-based polarization approach carried out in acid with stainless steel as cathode and platinum as counter electrode.

The hydrogen bubble formation plus electrodeposition of platinum were found to occur simultaneously on the surface of Ni42 steel upon carrying out repetitive CV scans in sulfuric acid. The HER disturbs homogeneous decoration of Ni42 steel with platinum. However, the latter is advantageous with respect to activity and stability of the generated HER electrode and can be achieved by ultrasonically treating the electrolytic cell. An optimized electrolysis protocol allows the generation of a very active ( $\eta = +140$  mV at  $j = -10$  mA cm<sup>-2</sup> and at pH 1) and stable steel-based hydrogen evolution electrode, which can be seen as highly cost-effective due to the low amount of used platinum (18  $\mu$ g mm<sup>-2</sup>). Remarkably, only a negligible amount of Pt (26  $\mu$ g) was determined in the electrolyte used for the platinum transfer reaction which means that around 99% of the Pt that comes from the Pt counter electrode is deposited on the WE, making this procedure an ideal alternative to usually exploited strategies.

## Acknowledgements

This research did not receive any specific grant from funding agencies in the public, commercial, or not-for-profit sectors.

## Conflict of interest

The authors declare no conflict of interest.

**Keywords:** electrocatalysis · heterogeneous catalysis · hydrogen evolution · water splitting

**How to cite:** *Angew. Chem. Int. Ed.* **2019**, *58*, 17383–17392  
*Angew. Chem.* **2019**, *131*, 17544–17553

- [1] F. Le Formal, W. S. Bouree, M. S. Prevot, K. Sivula, *Chimia* **2015**, *69*, 789–798.
- [2] T. R. Cook, D. K. Dogutan, S. Y. Reece, Y. Surendranath, T. S. Teets, D. G. Nocera, *Chem. Rev.* **2010**, *110*, 6474–6502.
- [3] M. G. Walter, E. L. Warren, J. R. McKone, S. W. Boettcher, Q. Mi, E. A. Santori, N. S. Lewis, *Chem. Rev.* **2010**, *110*, 6446–6473.
- [4] H. A. Gasteiger, N. M. Markovic, *Science* **2009**, *324*, 48–49.
- [5] S. Baranton, C. Coutanceau, *Appl. Catal. B* **2013**, *136–137*, 1–8.
- [6] X. Sun, K. Xu, C. Fleischer, X. Liu, M. Grandcolas, R. Strandbakke, T. S. Bjornheim, T. Norby, A. Chatzitakis, *Catalysts* **2018**, *8*, 1–41.
- [7] G. Yang, S. Yu, J. Mo, Z. Kang, Y. Dormann, F. A. List III, J. B. Green, S. S. Babu, F.-Y. Zhang, *J. Power Sources* **2018**, *396*, 590–598.
- [8] V. Artero, M. Chavarot-Kerlidou, M. Fontecave, *Angew. Chem. Int. Ed.* **2011**, *50*, 7238–7266; *Angew. Chem.* **2011**, *123*, 7376–7405.
- [9] V. R. Stamenkovic, D. Strmcnik, P. P. Lopes, N. M. Markovic, *Nat. Mater.* **2017**, *16*, 57–69.
- [10] C. Jorgensen, S. Ropenus, *Int. J. Hydrogen Energy* **2008**, *33*, 5335–5344.
- [11] J. Wang, W. Cui, Q. Liu, Z. Xing, A. M. Asiri, X. Sun, *Adv. Mater.* **2016**, *28*, 215–230.
- [12] C. C. L. McCrory, S. Jung, J. C. Peters, T. F. Jaramillo, *J. Am. Chem. Soc.* **2013**, *135*, 16977–16987.
- [13] J. G. Chen, C. W. Jones, S. Linic, V. R. Stamenkovic, *ACS Catal.* **2017**, *7*, 6392–6393.
- [14] H. Schäfer, M. Chatenet, *ACS Energy Lett.* **2018**, *3*, 574–591.
- [15] F. Moureaux, P. Stevens, G. Toussaint, M. Chatenet, *J. Power Sources* **2013**, *229*, 123–132.
- [16] H. Schäfer, S. Sadaf, L. Walder, K. Kuepper, S. Dinklage, J. Wollschläger, L. Schneider, M. Steinhart, J. Hardege, D. Daum, *Energy Environ. Sci.* **2015**, *8*, 2685–2697.
- [17] H. Schäfer, D. M. Chevrier, K. Kuepper, P. Zhang, J. Wollschläger, D. Daum, M. Steinhart, C. Heß, U. Krupp, K. Müller-Buschbaum, J. Stangl, M. Schmidt, *Energy Environ. Sci.* **2016**, *9*, 2609–2622.
- [18] H. Schäfer, K. Kuepper, J. Koppe, P. Selter, M. Steinhart, M. R. Hansen, D. Daum, *ACS Catal.* **2018**, *8*, 10914–10925.
- [19] H. Schäfer, K. Kuepper, M. Schmidt, K. Müller-Buschbaum, D. Daum, M. Steinhart, W. Han, J. Wollschläger, U. Krupp, P. Hou, J. Stangel, X. Liu, *Catal. Sci. Technol.* **2018**, *8*, 2104–2116.
- [20] D. Voiry, M. Salehi, R. Silva, T. Fujita, M. W. Chen, T. Asefa, V. B. Shenoy, G. Eda, M. Chhowalla, *Nano Lett.* **2013**, *13*, 6222–6227.
- [21] Y. Zhang, A. Thomas, M. Antonietti, X. Wang, *J. Am. Chem. Soc.* **2009**, *131*, 50–51.
- [22] B. G. Pollet, E. F. Valzer, O. J. Curnick, *Int. J. Hydrogen Energy* **2011**, *36*, 6248–6258.
- [23] B. G. Pollet, *Ultrason. Sonochem.* **2019**, *52*, 6–12.
- [24] M. H. Islam, O. S. Burheim, B. G. Pollet, *Ultrason. Sonochem.* **2019**, *51*, 533–555.
- [25] *Power Ultrasound in Electrochemistry: From Versatile Laboratory Tool to Engineering Solution* (Ed.: B. G. Pollet), Wiley, Hoboken, **2012**.
- [26] E. J. Popczun, C. G. Read, C. W. Roske, N. S. Lewis, R. E. Schaak, *Angew. Chem. Int. Ed.* **2014**, *53*, 5427–5430; *Angew. Chem.* **2014**, *126*, 5531–5534.

- [27] E. J. Popczun, J. R. McKone, C. G. Read, A. J. Biacchi, A. M. Wiltrout, N. S. Lewis, R. E. Schaak, *J. Am. Chem. Soc.* **2013**, *135*, 9267–9270.
- [28] Y.-Y. Ma, C.-X. Wu, X.-J. Feng, H.-Q. Tan, L.-K. Yan, Y. Liu, Z.-H. Kang, E.-B. Wang, Y.-G. Li, *Energy Environ. Sci.* **2017**, *10*, 788–798.
- [29] Z. Duan, M. Pi, D. Zhang, P. Zhang, J. Deng, S. Chen, *Int. J. Hydrogen Energy* **2019**, *44*, 8062–8069.
- [30] R. S. Vishwanath, S. Kandaiah, *J. Mater. Chem. A* **2017**, *5*, 2052–2065.
- [31] Z. Jin, P. Li, D. Xiao, *Green Chem.* **2016**, *18*, 1459–1464.
- [32] J. Hu, C. Zhang, X. Meng, H. Lin, C. Hu, X. Long, S. Yang, *J. Mater. Chem. A* **2017**, *5*, 5995–6012.
- [33] E. R. Gonzalez, L. A. Avaca, A. Carubelli, A. A. Tanaka, G. Tremiliosi-Filho, *Int. J. Hydrogen Energy* **1984**, *9*, 689–693.
- [34] K. C. Leonard, M. I. Tejedor-Anderson, M. A. Anderson, *Int. J. Hydrogen Energy* **2012**, *37*, 18654–18660.
- [35] S. Wang, W. Li, H. Qin, L. Liu, Y. Chen, D. Xiang, *Int. J. Electrochem. Sci.* **2019**, *14*, 957–969.
- [36] G. Cabello, M. F. Gromboni, E. C. Pereira, L. H. Mascaro, F. Marken, *Electrochim. Acta* **2017**, *235*, 480–487.
- [37] T. Zhang, K. Yang, C. Wang, S. Li, Q. Zhang, X. Chang, J. Li, S. Li, S. Jia, J. Wang, L. Fu, *Adv. Energy Mater.* **2018**, *8*, 1801690.
- [38] J. M. Olivares-Ramírez, M. L. Campos-Cornelio, J. Uribe Godínez, E. Borja-Arco, R. H. Castellanos, *Int. J. Hydrogen Energy* **2007**, *32*, 3170–3173.
- [39] A. Fones, G. Hatton, *Platinum Met. Rev.* **2014**, *58*, 54–57.
- [40] H. Schäfer, D. M. Chevrier, P. Zhang, J. Stangl, K. Müller-Buschbaum, J. D. Hardege, K. Kuepper, J. Wollschläger, U. Krupp, S. Dühren, M. Steinhart, L. Walder, S. Sadaf, M. Schmidt, *Adv. Funct. Mater.* **2016**, *26*, 6402–6417.
- [41] W. Han, K. Küpper, P. Hou, W. Akram, H. Eickmeier, J. Hardege, M. Steinhart, H. Schäfer, *ChemSusChem* **2018**, *11*, 3661–3671.
- [42] Q. Yuan, Y. Wakisaka, Y. Uemura, T. Wada, H. Ariga-Miwa, S. Takakusagi, K. Asakura, S. R. Brankovic, *J. Phys. Chem. C* **2018**, *122*, 16664–16673.
- [43] K. S. Kim, N. Winograd, R. E. Davis, *J. Am. Chem. Soc.* **1971**, *93*, 6296–6297.
- [44] R. Arrigo, M. Hävecker, M. E. Schuster, C. Ranjan, E. Stotz, A. Knop-Gericke, R. Schlögl, *Angew. Chem. Int. Ed.* **2013**, *52*, 11660–11664; *Angew. Chem.* **2013**, *125*, 11874–11879.
- [45] V. A. Saveleva, V. Papaefthimiou, M. K. Daletou, W. H. Doh, C. Ulhaq-Bouillet, M. Diebold, S. Zafeiratos, E. R. Savinova, *J. Phys. Chem. C* **2016**, *120*, 15930–15940.
- [46] J. P. Hoare in *Advances in Electrochemistry and Electrochemical Engineering, Vol. 6* (Eds.: P. Delahay, C. W. Tobias), Interscience, New York, **1966**, pp. 201–288.
- [47] C. C. Tseung, S. Jasem, *Electrochim. Acta* **1977**, *22*, 31–34.
- [48] M. Pourbaix in *Atlas d'Equilibres Electrochimiques a 25 8C*, Gauthiers-Villars, Paris, **1963**.
- [49] H. Angerstein-Kozłowska, B. E. Conway, B. Barnett, J. Mozota, *J. Electroanal. Chem.* **1979**, *100*, 417–446.
- [50] B. E. Conway, G. Tremiliosi-Filho, G. Jerkiewicz, *J. Electroanal. Chem.* **1991**, *297*, 435–443.
- [51] B. E. Conway, G. Jerkiewicz, *J. Electroanal. Chem.* **1992**, *339*, 123–146.
- [52] B. E. Conway, *Prog. Surf. Sci.* **1995**, *49*, 331–452.
- [53] S. Mitsushima, Y. Koizumi, S. Uzuka, K.-I. Ota, *Electrochim. Acta* **2008**, *54*, 455–460.
- [54] M. Tian, C. Cousins, D. Beauchemin, Y. Furuya, A. Ohma, G. Jerkiewicz, *ACS Catal.* **2016**, *6*, 5108–5116.
- [55] R. M. Darling, J. P. Meyers, *J. Electrochem. Soc.* **2003**, *150*, A1523–A1527.
- [56] S. A. Grigoriev, P. Millet, V. N. Fateev, *J. Power Sources* **2008**, *177*, 281–285.
- [57] M. Bernt, A. Siebel, H. A. Gasteiger, *J. Electrochem. Soc.* **2018**, *165*, F305–F314.
- [58] L. Dubau, L. Castanheira, G. Berthomé, F. Maillard, *Electrochim. Acta* **2013**, *110*, 273–281.
- [59] L. Dubau, M. Lopez-Haro, L. Castanheira, J. Durst, M. Chatenet, P. Bayle-Guillemaud, L. Guétaz, N. Caqué, E. Rossinot, F. Maillard, *Appl. Catal. B* **2013**, *142–143*, 801–808.
- [60] Z. Zhao, L. Castanheira, L. Dubau, G. Berthomé, A. Crisci, F. Maillard, *J. Power Sources* **2013**, *230*, 236–243.
- [61] L. Castanheira, L. Dubau, F. Maillard, *Electrocatalysis* **2014**, *5*, 125–135.
- [62] L. Castanheira, L. Dubau, M. Mermoux, G. Berthomé, N. Caqué, E. Rossinot, M. Chatenet, F. Maillard, *ACS Catal.* **2014**, *4*, 2258–2267.
- [63] L. Dubau, L. Castanheira, M. Chatenet, F. Maillard, J. Dillet, G. Maranzana, S. Abbou, O. Lottin, G. De Moor, A. El Kaddouri, C. Bas, L. Flandin, E. Rossinot, N. Caqué, *Int. J. Hydrogen Energy* **2014**, *39*, 21902–21914.
- [64] L. Dubau, L. Castanheira, F. Maillard, M. Chatenet, O. Lottin, G. Maranzana, J. Dillet, A. Lamibrac, J.-C. Perrin, E. Moukheiber, A. ElKaddouri, G. De Moor, C. Bas, L. Flandin, N. Caqué, *WIRES Energy Environ.* **2014**, *3*, 540–560.

Manuscript received: July 11, 2019

Accepted manuscript online: September 20, 2019

Version of record online: October 15, 2019